3D FEM approach for laterally loaded monopile design

Murphy, Gerry; Igoe, David; Doherty, Paul; Gavin, K.

DOI
10.1016/j.compgeo.2018.03.013

Publication date
2018

Document Version
Final published version

Published in
Computers and Geotechnics

Computers and Geotechnics 100 (2018) 76–83

Contents lists available at ScienceDirect

Computers and Geotechnics

journal homepage: www.elsevier.com/locate/compgeo

Research Paper

3D FEM approach for laterally loaded monopile design

Gerry Murphy[a], David Igoe[a,b,*], P. Doherty[a], K. Gavin[a,c]

[a] Gavin and Doherty Geosolutions, Dublin, Ireland
[b] Trinity College Dublin, Ireland
[c] TU Delft, The Netherlands

ARTICLE INFO

Keywords:
Offshore foundations
Piling
Lateral loading
Finite element modelling
Monopiles

ABSTRACT

Over the past 5 years, a substantial research effort aimed at optimising the design of offshore wind turbines has led to significant reductions in the projected cost of developing offshore wind. Optimising the geotechnical design of these structures, through modern analysis techniques such as 3D Finite Element Modelling (FEM), has played a key role in helping to reduce costs. This paper presents a methodology for accurately modelling monopile behaviour using Cone Penetration Test (CPT) data to calibrate the non-linear stress dependent Hardening Soil (HS) model. The methodology is validated by comparing the modelled behaviour to field tests on a range of pile geometries. The paper also demonstrates how the soil-pile reaction response curves can be extracted from the FE model by isolating the stresses on each element of the pile. The contribution of each component to the overall lateral resistance is shown to vary with the pile geometry and is examined using the extracted soil reaction curves.

1. Introduction

Monopiles are the most commonly used foundation system for supporting offshore wind turbines, accounting for ~80% of all sub-structures installed to date [1]. Monopile foundations are single large diameter open-ended tubular steel piles, typically driven into the sea bed, which rely on the stiffness and strength of the surrounding soil to provide resistance against large environmental loads from wind and waves. Typical monopile diameters range from 4 to 6 m, however due to increasing turbine sizes and applicable water depths, XXL monopiles of up to 10 m in diameter are being considered [2]. The slenderness ratio of embedded pile length to diameter (L/D) of a monopile typically varies between 4 and 8, depending on the applied loading and ground conditions, but L/D ratios of 3 or less are anticipated for future XXL monopiles.

1.1. Monopile design practice

The traditional industry standard approach for the geotechnical design of monopiles are those recommended by Det Norske Veritas – Germanischer Lloyd (DNV-GL), which are based on American Petroleum Institute (API) design guidelines, and were originally intended for oil & gas jacket piles. Both guidance documents adopt a Winkler beam approach where the lateral soil reaction at a given depth is described by decoupled non-linear 'p-y' curves, where p is the lateral soil reaction and y is the lateral displacement response [3,4]. The methods were calibrated using a limited number of pile tests performed on slender jacket piles with diameters less than 1 m, and are generally not valid for large diameter monopiles. Recent editions of the DNV-GL guidelines have been updated to recommend that the p-y curves used for monopile design should be validated by FE analysis, however currently there is no consensus on how this is best achieved in practice.

For the geotechnical design of an individual monopile, a number of limit states must be considered. This paper focuses on the Ultimate Limit State (ULS) and Serviceability Limit State (SLS) pile behaviour as the design pile length is typically governed by these cases. For each individual turbine, a significant number of load cases must be analysed, including time domain analyses for the dynamic response during operation [5]. In addition, the calculated loading is dependent on the structures geometry and the foundation stiffness and therefore requires a number of load-geometry iterations for optimisation. The use of numerical approaches, such as 3D FEM, are now widely adopted in both research and industry for modelling complex 3D soil-structure interaction problems. However, when considering the optimisation of an entire offshore wind farm, it becomes clear that relying solely on 3D FEM is too computationally expensive for running all the necessary design iterations and therefore simpler Winkler beam type models are still required [6].

* Corresponding author at: Trinity College Dublin, Ireland.
E-mail address: igoed@tcd.ie (D. Igoe).

https://doi.org/10.1016/j.compgeo.2018.03.013
Received 17 August 2017; Received in revised form 21 February 2018; Accepted 27 March 2018
Available online 13 April 2018

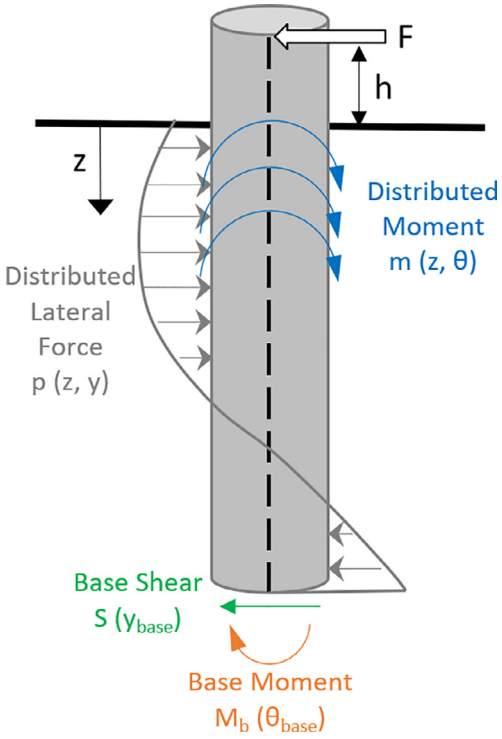

Fig. 1. Soil reaction curves after [2].

1.2. Current state of the art in monopile geotechnical design

In order to reduce calculation times and improve design efficiency Byrne et al. [2] proposed that the soil reaction curves can be extracted from 3D FE analyses and implemented in a 1D spring model [5]. This method benefits from both the accurate model complexity provided by the 3D FEM and also the reduced computation time of the conventional p-y framework. In order to achieve an accurate representation of the 3D FEM using a 1D Winkler beam model, Byrne et al. [2] extended the traditional 'p-y' approach to include additional soil reaction components as follows: (i) the distributed moments, m, due to vertical shaft shear stresses during pile rotation at given depth θ; (ii) the base shear, S, during horizontal translation at the pile toe and (iii) the base moment, M, during rotation of the pile toe, see Fig. 1 [2]. These additional components of soil reaction have been shown to have a significant influence on Monopiles with a slenderness ratio (L/D) of less than 5. The methodology outlined in this paper shows how each soil reaction component can be extracted from a 3D FE Plaxis model, and used as inputs to a 1D FE model to quickly optimise the monopile design and improve design efficiency.

It should be noted that the potential of this approach is entirely dependent on developing 3D FE models which can reliably and accurately capture the monopile response under a range of loading conditions covering small to large strains. To date several studies have been published in which large diameter monopiles have been successfully analysed using commercially available 3D FE packages [7–15], however few have been validated against actual monopile load test results and therefore the accuracy of these models is uncertain.

The calibration of the constitutive soil model to accurately capture the non-linear behaviour over a large strain range is the key challenge when modelling the monopile response. In this paper, the Hardening Soil (HS) soil model was chosen because of its ability to model non-linear soil behaviour, but also for the simplicity of deriving the model input parameters. Several more advanced constitutive soil models, which have the ability to better capture the fundamental critical state mechanics of sands and clays, have been utilised for predicting the behaviour of laterally loaded piles in recent studies [16–19]. However, there is often an inherent difficulty in using these models in practice due to difficulties in calibrating the input parameters which, in some cases, require significant specialised laboratory element testing.

For most offshore wind farms, only a limited amount of geotechnical information will be available at an early stage of a project, typically CPT tests and a limited amount of standard laboratory tests (shear box, triaxial, oedometer, DSS). In addition, the difficulty in acquiring undisturbed sand samples offshore means that these lab tests are often carried out on reconstituted samples and may not be representative of the particle interlocking, cementation and dilatational behaviour of aged dense sand deposits in-situ. Therefore, using a relatively simple constitutive model which can capture the non-linear soil response (such as the HS model) and which can be calibrated using in-situ test data such as CPT tests offers a useful way for designers to estimate the monotonic pile loading response.

2. 3D FE modelling

2.1. General modelling approach

The monopile field tests described in this paper were modelled using the commercially available Plaxis 3D 2013 software. The axisymmetric nature of the problem was not considered and a full mesh was used with the pile positioned at the centre of the mesh. The finite element mesh used in the analysis is shown in Fig. 2. The lateral boundary was set at forty pile diameters and the depth was set as twice the embedded pile length. The soil elements were modelled as ten-node tetrahedral elements. The pile wall was modelled as an 18 sided cylindrical plate using six-node plate elements, see Table 1 for number of nodes and elements in each model. The mesh was generated using the inbuilt Plaxis meshing procedure and was refined until a satisfactory mesh quality index was achieved. The piles were modelled as linear elastic elements with Youngs Modulus, E_p = 200 GPa, Poisson's ratio, υ_p = 0.3 and a unit weight of γ = 77 kN/m^3. Interface elements were also added to the pile shaft. The reduction in interface shear strength when slip occurs is accounted for using the strength reduction factor R_{inter} = 0.7 which was in agreement with previous studies at the test site [20]. It should be noted that site specific calibration of all parameters including the shear strength reduction factor is essential for accurate modelling of the soil-pile system. In order to account for pile installation affects and the increased stresses in the vicinity of the pile base as a result of 'locked-in' residual loads developed during pile driving, a vertical jacking phase was applied to the 3D FE model pile prior to application of the lateral loading phases. The use of a jacking phase to model installation effects is described in greater detail in Section 4.

2.2. Development of soil model

The field tests were modelled using commercially available finite element software Plaxis 3D – 2013. The HS model, as described by

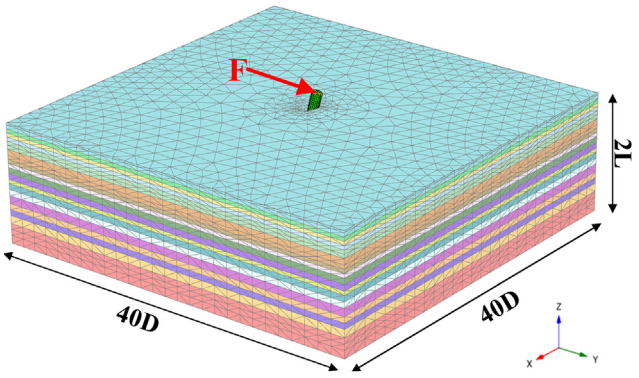

Fig. 2. Typical mesh used in pile analysis.

Table 1
Monopile test pile dimensions.

		Units	P1	P2	P3	P4
Embedded length	L	mm	1500	1500	2250	3000
Diameter	D	mm	245	510	510	510
Wall thickness	T	mm	8	10	10	10
L/D ratio	–	–	6	3	4	6
Load eccentricity	h	mm	400	1000	1000	1000
Test location	–	–	Upper	Lower	Lower	Lower
FEM – nodes	–	–	69,367	139,407	156,147	148,137
FEM – elements	–	–	47,218	95,865	103,795	100,355

Schanz [21], was adopted to define the soil stiffness behaviour. The HS parameters were derived using correlations with the CPT cone resistance (q_c) at both sites. The first step in the design process was the discretisation of the CPT profiles for the upper and lower level test sites, as shown in Fig. 3a. The peak friction angle, φ, was estimated accounting for density and stress level effects using Eqs. (1)–(3) [22–24].

$$\varphi = 17.6 + 11\log\left[\left(\frac{q_t}{P_a}\right)/\left(\frac{\sigma'_{vo}}{P_a}\right)\right]^{0.5} \quad (1)$$

$$\psi = (\varphi - \varphi'_{cv})/0.8 \quad (2)$$

$$D_r^2 = \frac{\frac{q_c}{P_a}}{350\left(\frac{\sigma'_{vo}}{P_a}\right)^{0.5}} \quad (3)$$

where q_t is the cone tip stress corrected for pore water effects, σ'_{vo} is the effective vertical stress ($\sigma'_{vo} = \sigma'_1$) calculated using an effective unit weight of 20 kN/m^3, P_a is the reference atmospheric pressure (=100 kPa), ψ is the dilation angle, φ'_{cv} is the constant volume friction angle calculated from simple laboratory tests and D_r is the relative density (%). The in-situ soil stress state calculated using Eqs. (4)–(6) [25,26].

$$OCR = \left[\frac{1.33 * q_t^{0.22}}{K_{0NC} * \sigma_{vo}^{0.31}}\right]^{\frac{1}{\sin\varphi - 0.27}} \quad (4)$$

$$K_{0NC} = 1 - \sin\varphi \quad (5)$$

$$K_0 = K_{0NC} * OCR^{\sin\varphi} \quad (6)$$

where OCR is the overconsolidation ratio of the soil, K_{0NC} is the lateral stress coefficient for normally consolidated soils and K_0 describes the effect of OCR on the lateral stress coefficient [27].

The stiffness characteristics of the HS model were defined for each layer based on the empirical correlations for the constrained tangent stiffness modulus E_{oed} from Kulhawy & Mayne (1990), the secant stiffness modulus E_{50} was calculated using Hooke's law as described by Brinkgreve et al. (2012) [27,28].

$$E_{oed,NC} = q_c 10^{1.09 - 0.0075 D_r} \quad (7)$$

$$E_{oed,OC} = q_c 10^{1.78 - 0.0122 D_r} \quad (8)$$

$$E_{50} = \frac{(1-2\nu)(1+\nu)}{1-\nu} E_{oed} \quad (9)$$

$$E_{ur} = 3 \times E_{50} \quad (10)$$

where $E_{oed,NC}$ and $E_{oed,OC}$ are the constrained tangent oedometer modulus for normally and over consolidated sands, E_{50} is the secant stiffness modulus calculated following Hooke's law and E_{ur} is the unload-reload stiffness calculated as recommended in the Plaxis materials manual. As the sand at the Blessington site is overconsolidated, Eq. (8) was adopted to derive the E_{oed} value. These moduli are dependent on the in-situ stress following the shape of the power function, m, given in Brinkgreve et al. (2012) and are inputted into Plaxis 3D as reference values (Pa = 100 kPa). The reference moduli are calculated as follows:

$$E_{oed}^{ref} = E_{oed} / \left(\frac{c\cos\varphi - \frac{\sigma'_3}{K_{0NC}}\sin\varphi}{c\cos\varphi + P_a \cdot \sin\varphi}\right)^m \quad (11)$$

$$E_{50}^{ref} = E_{50} / \left(\frac{c\cos\varphi - \sigma'_3\sin\varphi}{c\cos\varphi + P_a \cdot \sin\varphi}\right)^m \quad (12)$$

$$E_{ur}^{ref} = E_{ur} / \left(\frac{c\cos\varphi - \sigma'_3\sin\varphi}{c\cos\varphi + P_a \cdot \sin\varphi}\right)^m \quad (13)$$

where the exponent m defines the stress dependent stiffness and c is the effective cohesion. Brinkgreve et al. (2012) recommends a value of m = 0.5 for sands and silts. The constant parameters used in the hardening soil model for this site are presented in Table 2 and Fig. 3 presents the cone resistance profile and the interpreted soil stiffness parameters.

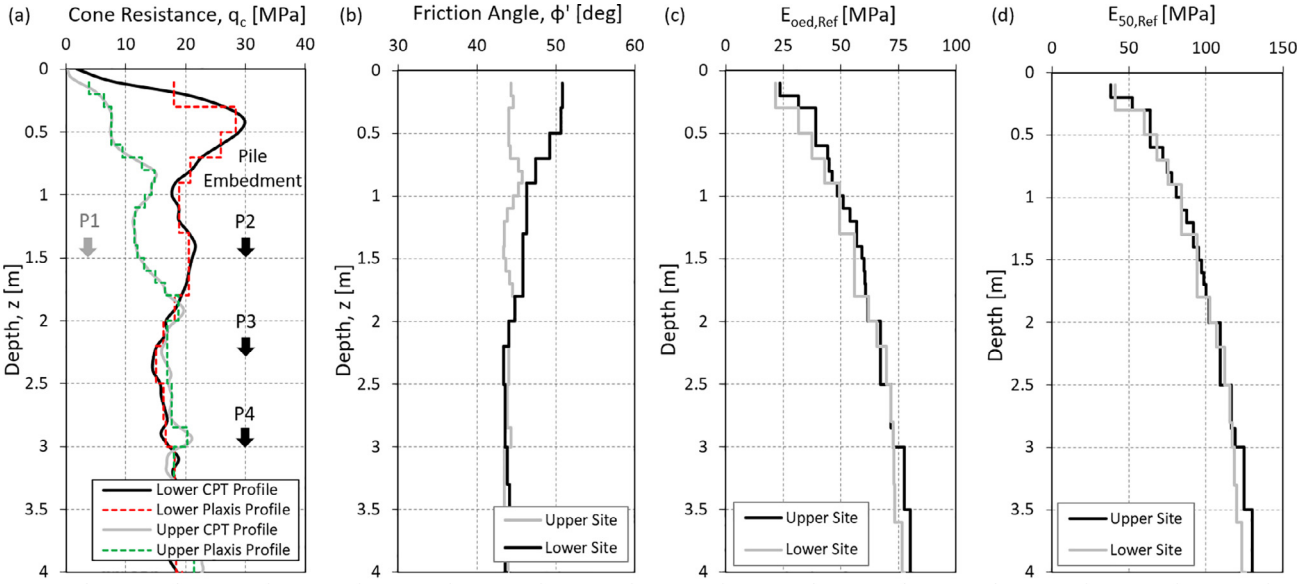

Fig. 3. (a) CPT Profile (b) Peaks Shear Friction Angle (c) & (d) Reference Tangent and Secant Stiffness at 100 kPa.

Table 2
Constant soil model inputs.

Parameter	Symbol	Units	Value
Effective soil weight	γ	kN/m^3	20
Effective cohesion	c′	kN/m^2	0.1
Reference stress	P_a	kN/m^2	100
Poissons ratio	ν	–	0.2
Void ratio	e_{max}	–	0.91
	e_{min}	–	0.57
Interface Stiffness	R_{inter}	–	0.7

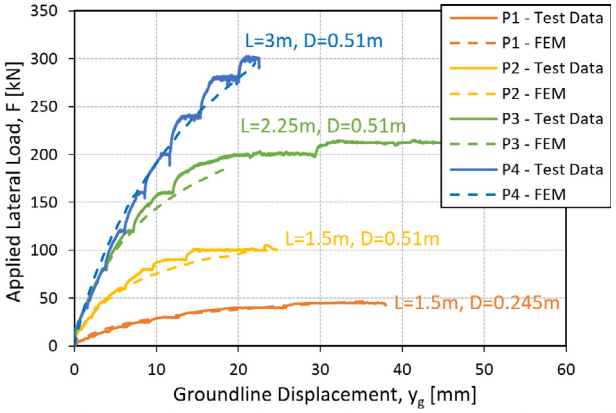

Fig. 4. Load-displacement response of test piles compared to model results.

2.3. Post processing soil reaction curves

Soil reaction curves can be extracted from the 3D FE model for future application into a less computationally intensive 1D spring model. The soil reaction curves can be calculated by examining the stresses acting on the pile structural elements, following the methodologies of [2,10,16]. For each loading stage, the stresses acting on the pile interface elements are outputted at fixed stress points as effective normal stresses and horizontal and vertical shear stresses. The stresses at each gauss point along the pile circumference are resolved into resultant forces acting in the loading (y) direction using Gaussian quadrature. The angle of the each stress relative to the y-direction in the horizontal plane is determined from the coordinates of the node points from the corresponding pile plate elements. The total area of each plate element is determined as the cross product of the corner node coordinates, and the appropriate Gaussian weight factor is applied to each stress point based on the stress point nomenclature, as defined in [28].

The soils distributed reaction force in the y-direction, p, is then calculated at the midpoint of each discretisation depth by summing all the resolved lateral forces acting on the external pile surface over the discretisation interval. Likewise, the distributed moment, m, is calculated from the vertical shear forces acting around the pile centreline. The base shear and base moment are calculated in a similar manner from the stresses acting on the internal pile shaft. The profiles of horizontal pile displacement (y) with depth (z) are extracted from the plate elements within Plaxis 3D by generating load-displacement curves at fixed depths corresponding to the mid-point of the elements along the pile for each load stage.

This process is repeated for each discretisation depth and automated using a code implemented in Matlab to reduce calculation time. The forces in the load direction and bending moments along the pile circumference are then used to create bending moment and shear force profiles along the pile shaft. The bending moments along the length of the pile can be calculated from the extracted soil stresses by double integration of the lateral forces (in the y-direction) on the external pile surface, p, and the equivalent forces on the internal pile surface, s. These are then combined with the distributed moments due to the vertical shear stress acting on the internal and external pile faces as in Eq. (14).

$$M_z = F{\cdot}(h+z) + \iint_0^z (p+s){\cdot}dz + \int_0^z (m+m_{int}){\cdot}dz \tag{14}$$

where M_z is the bending moment at depth below mudline z, F is the applied load above mudline, h is the height of load application above mudline, m is the distributed moment due to vertical shear forces on the external pile surface and m_{int} is the distributed moment due to vertical shear forces on the internal pile surface. To develop the additional reaction springs proposed by Byrne et al. to be implemented in a Winkler beam model, the base shear – displacement, S-y, and base moment-rotation, M_b-θ, can be calculated as:

$$S = \int_0^L s{\cdot}dz \tag{15}$$

$$M_b = \int_0^L m_{int}{\cdot}dz \tag{16}$$

where L is the pile embedded length. Equilibrium can be checked by comparing the sum of the forces and moments in the load direction to the applied load. A moment equilibrium tolerance of less than 1% was achieved in this study.

3. Field testing

3.1. Monopile static loading field tests

To validate the FE models, a series of field tests were conducted using prototype scale piles embedded in an over-consolidated dense sand deposit. Four open-ended steel piles with diameters of 245 mm and 510 mm were driven to embedded lengths between 1500 mm and 3000 mm (with slenderness ration, L/D, between 3 and 6), see Table 1. The piles were installed at two locations in an active quarry. The first (upper) location was excavated more than ten years before the load tests were performed. The second (lower) location was excavated more recently.

The test site is located in Blessington, approximately 25 km southwest of Dublin in Ireland. The site consists of a uniformly graded, horizontally bedded, heavily over-consolidated, and very dense sand deposit. An extensive site investigation comprising CPT, Seismic Dilatometer Testing (SDMT), plate load testing, sonic core sampling, trial pits (for soil classification testing), and in-situ geophysical testing have been undertaken and detailed descriptions of soil properties have been described in previous publications, see [20,29–31]. The water table is > 10 m below ground level (bgl) at the upper site and 2.5 m bgl. at the lower site. The CPT q_c profiles shown in Fig. 3(a) reveal that the q_c values are notably larger over the top 2 m bgl at the lower site. At depths greater than 2 m bgl, the profiles become very similar. Test pile P1 was instrumented using strain gauges attached to the tension and compression faces of the pile. The strain gauge data was used to derive bending moment profiles for each load increment applied in a static load test as described in detail by Xue et al. and Murphy et al. [32,33]. The test piles were loaded (using maintained load increments) until pile head displacement continued without the addition of a further load increment. The test configuration used for the 510 mm pile was similar to the 245 mm tests described in Murphy et al., however, a load eccentricity of 1 m was used, compared with an eccentricity of 0.4 m for the 245 mm pile tests. The test load was measured using an in-line load cell, the lateral displacement of the test piles was measured at three locations using linear displacement transducers and the pile rotation was measured using four digital inclinometers. The measured load-displacement response of the field test piles are presented in Fig. 4 (solid lines).

4. Analysis and 3D FE model validation

Once each model run was completed, the load-displacement and soil reaction curves were extracted from each load stage using the displacement and stresses acting along the pile shaft, following the procedure outlined previously. A comparison of the Plaxis model outputs with the field tests is shown in Fig. 4 which demonstrates the excellent agreement between the FEM displacements and the measured ground line displacements for all piles.

4.1. Consideration of installation stresses

The bearing capacity and stiffness response of a pile in sand is primarily dependent on the sand density and the in-situ stress state. Pile installation by driving will result in large shear strains and a significant increase in stress along the shaft and near the pile tip. These changes will increase the lateral bearing capacity and are critically dependent on the degree of plugging experienced by the pile during installation, see [31,34]. Most current numerical studies do not take installation effects into account, however some recent studies have examined this issue in detail and with some success using more advanced constitutive soil models [35,36].

Gavin and Lehane (2005) observed that the average base stress mobilised during a hammer blow is in the range of 10–20% of the q_c value [37]. When pile driving ceases a residual stress will remain at the pile tip, resulting in 'locked-in' stress in the vicinity of the pile base. Despite the increase in sophistication and computational power of commercially available FEM software most FEM codes do not permit the full simulation of the pile installation and the piles are simply

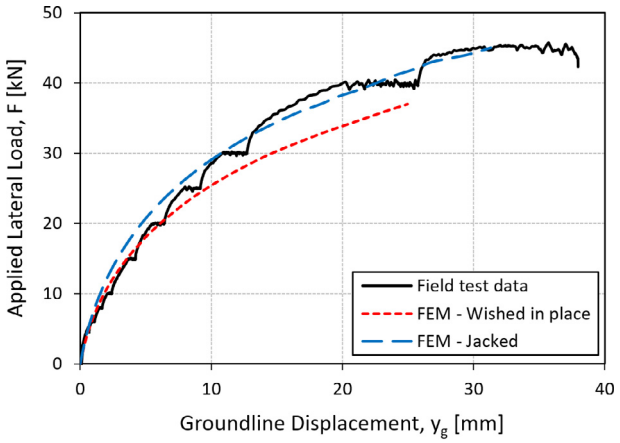

Fig. 6. Comparison of field tests results and modelled pile behaviour for pile P1.

"wished in place" with only the overburden stresses acting on the pile. This is due to large mesh distortion issues when considering large deformations [36,38]. In this paper, a hybrid approach was adopted to approximate the residual base stresses generated during pile driving. Firstly, the pile is "wished in place", then a series of vertical displacements were applied to the pile head to push (or jack) the pile a small distance into the soil mesh. Small vertical displacement increments (≈1%D) were used to approximate the final stages of pile driving. The stresses at the pile base were examined at each displacement stage. Due to the uncertainty over the residual forces locked into field piles after driving, and the difficulties in measuring and separating the internal

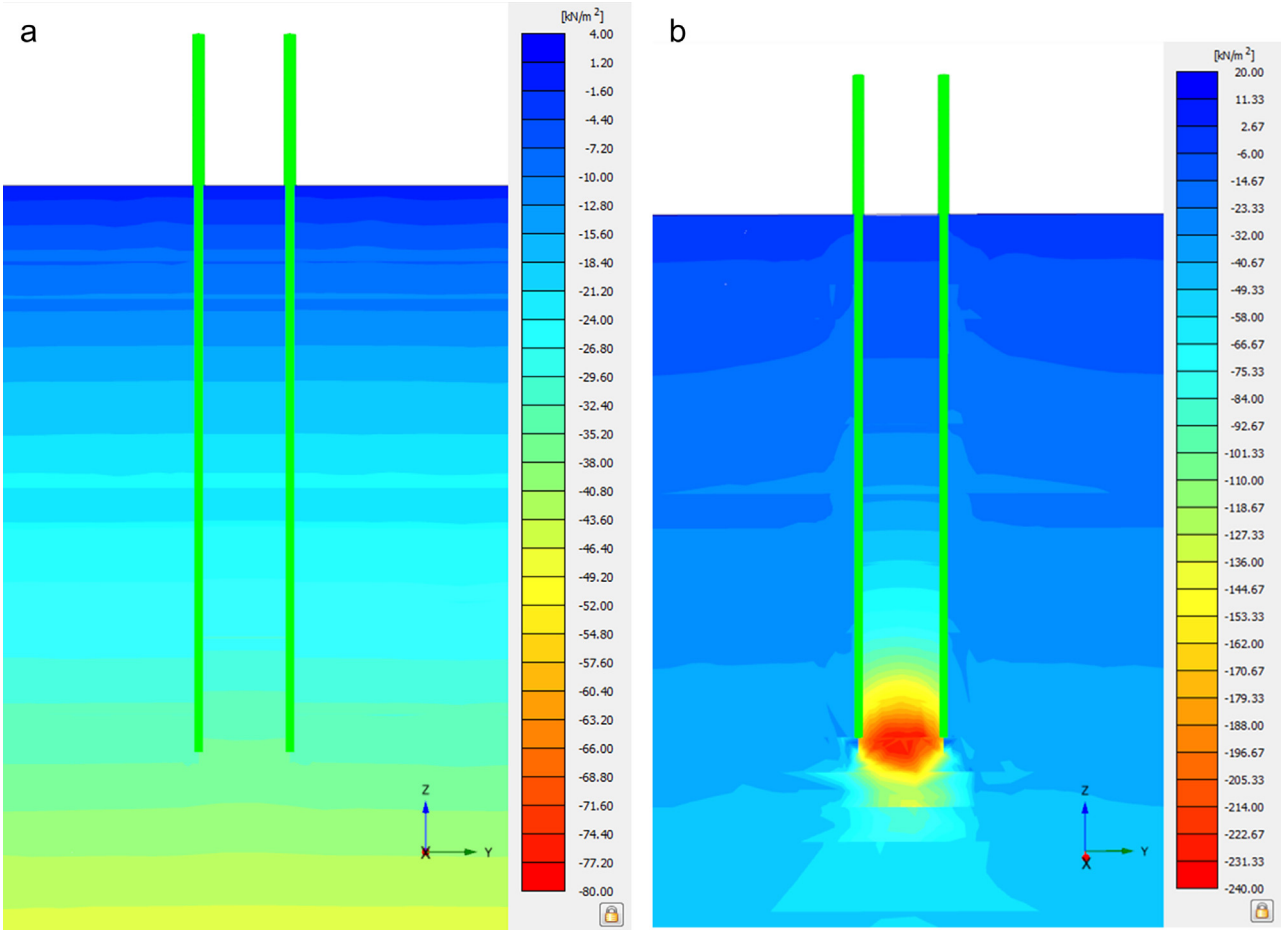

Fig. 5. Mean effective stresses p′ (a) prior to jacking stage (b) after jacking stage for pile P1.

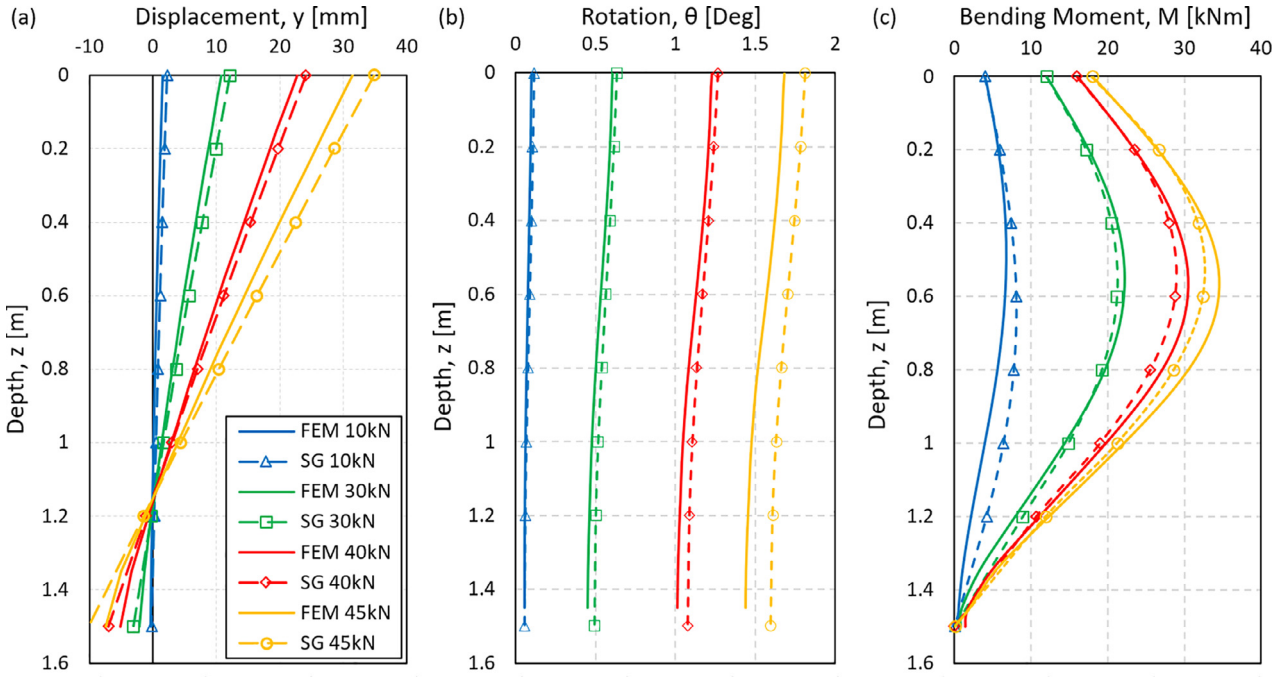

Fig. 7. Comparison of measured and predicted displacement, rotation and bending moment profiles for pile P1.

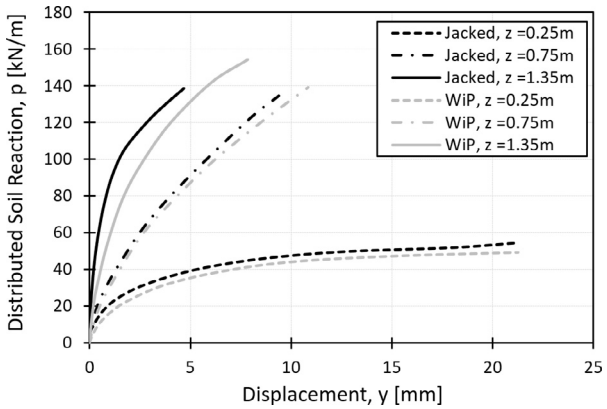

Fig. 8. Comparison of "Jacked" and "Wished-in-Place" FE models for pile P1 p-y response.

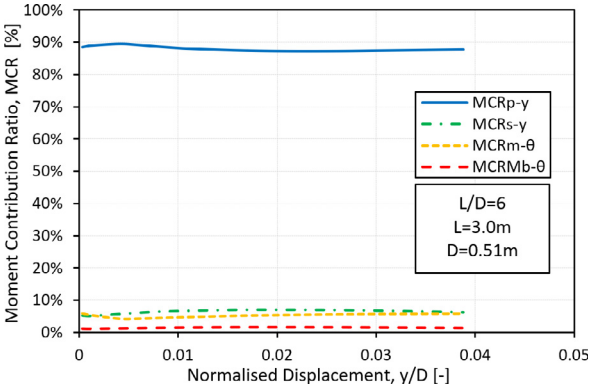

Fig. 9. Contribution of each resistance component for pile P2.

and external shaft friction of field piles, an approximation of the stress increase caused by pile driving was made. As an initial test, the vertical head displacement was increased in increments until an approximate ten-fold increase in mean effective stress (p′) was obtained numerically at the pile base, see Fig. 5. The models were then reset and the pile was wished in place, the chosen vertical displacement (to achieve the ten-fold increase in p′) was then applied prior to the lateral loading being applied. The resulting vertical stress at the base corresponded to approximately 15–20 times the in-situ vertical stress, σ'_{v0}, or around 2–5% of the CPT cone resistance, q_c, which was deemed to be an appropriate estimate of the residual base stress for an open-ended pile. The same process was applied to each model pile with consistent results.

The benefits of applying a jacking stage in capturing the overall pile response is shown for pile P1 in Fig. 6. It is evident that applying the jacking stage provides a better match to the overall pile response, albeit slightly over-predicting the initial stiffness. In practice, for full scale offshore wind turbine design, there will typically be a sizeable vertical load component due to the self-weight of the wind turbine structure, which should be included in any FE model. For a conservative (i.e. less stiff) design at full scale, it may be appropriate to include the vertical load component only.

The modelling approach was further validated by comparing the calculated pile shaft bending moments in P1 to those measured using strain gauges as shown in Fig. 7 [33]. A comparison of sample p-y curves extracted from the pile P1 "Jacked" and "Wished-in-Place" models are provided in Fig. 8. It is evident that applying a jacking stage only has a minor influence on the p-y curves at shallow and mid-depths, but significantly affects the p-y curves in the high stress zone near the pile toe.

4.2. Effect of slenderness ratio on soil reaction components

To gain a better understanding of the effect of pile slenderness ratio (L/D) on the relative contribution of the different soil resistance components, the contribution of each component was calculated as a percentage of the applied moment around the point of rotation (equal to the restoring moment exerted by the soil on the pile). The total moment contribution from the p-y and base shear components (i.e. force components) were calculated by multiplying the component force at each depth interval by its distance from the point of rotation (i.e. point of zero lateral displacement, calculated during each load step) and summing the calculated moments together for each component. The contribution due the distributed moment caused by vertical shaft shear

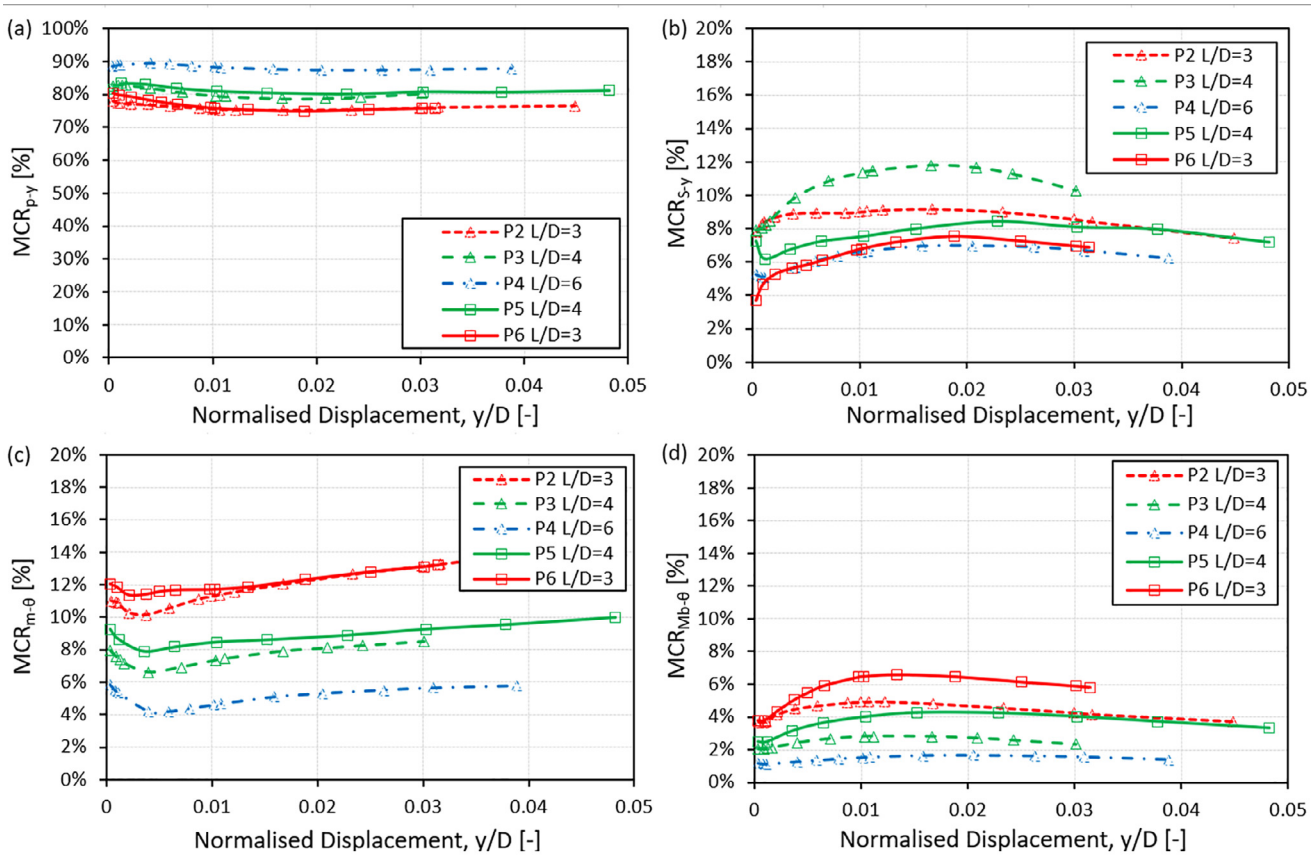

Fig. 10. Contribution of resistance components for each pile.

forces was calculated by integrating the distributed moment, m, along the length of the pile shaft. The total moments calculated from each of the soil reaction components was then divided by the externally applied moment (= applied lateral force × vertical distance to point of rotation) to calculate the 'Moment Contribution Ratio' (MCR).

The MCR values provided by each soil reaction component for pile P4 are shown in Fig. 9. The comparison shows that ~90% of the restoring moment comes from the distributed lateral load (MCR_{p-y}) acting along the pile shaft and that the MCR_{p-y} is relatively constant with displacement (i.e. from small to large strains). The moment contribution due to the shear force at the pile base (MCR_{S-y}), vertical stresses acting on the pile shaft ($MCR_{m-\theta}$), base moment ($MCR_{Mb-\theta}$) have a combined contribution of approximately 10%.

Further modelling was conducted to examine the influence pile geometries larger than those used in the prototype tests. Additional analyses were performed on pile P5 (L = 3, D = 0.76, L/D = 4) and P6 (L = 3, D = 1.02, L/D = 3). The relative contribution of each soil resistance component was compared for each L/D ratio in Fig. 10. Comparing the percentage contribution of each of the resistance components across the normalised displacement range, y/D, shows that as the L/D ratio decreased, the contribution of the lateral soil reaction MCR_{p-y} also reduced (Fig. 10a). As the L/D ratio of the piles reduced, the second order resistance components appeared to make a greater contribution to the stiffness response of the foundation (Fig. 10b–d). This is generally in agreement with recent research [2,5,6,39].

5. Conclusions

A methodology for predicting the displacement of laterally loaded monopile foundations using a commercially available finite element code is presented. The modelling procedure was validated by comparing the modelled load-displacement behaviour to the results of a series of field tests on prototype scale monopiles. Pile-Soil stresses obtained from the 3D FE model were analysed and used to obtain site-specific soil reaction curves for each pile.

An initial analysis of the pile resistance components is presented and the following conclusions were drawn:

- The comparison shows that ~75–90% of the restoring moment from the soil acting on the pile comes from the distributed lateral load (MCR_{p-y}) along the pile shaft for the range of pile geometries and applied loads considered.
- As the L/D ratio of the piles reduced, the second order resistance components make a larger contribution to the ultimate moment resistance of the foundation, in agreement with other researchers.
- The additional (non p-y) soil reaction components when combined can account for 10–25% of the moment resisted by the pile depending on the L/D ratio. Ignoring these effects may result in an overly conservative pile design for low slenderness monopiles (L/D < 6) which is in agreement with other researchers.

The advantage of the proposed methodology is that the modelling procedure can be completed relatively quickly using design inputs that are available in the majority of commercial offshore wind projects. This is particularly useful where it is difficult to obtain reliable undisturbed samples from offshore sites.

Acknowledgements

The authors would like to acknowledge the support of the Irish Research Council Employment-Based Postgraduate Programme, Roadstone Ltd. Blessington for access to the test sites and plant and Darren Ward at In-situ SI for conducting the CPT. We would also like to acknowledge the support of the EU funded project LEANWIND.

References

[1] Ewea. The European offshore wind industry. Key Trends Stat 2016; 2017, 33.
[2] Byrne BW, Mcadam R, Burd HJ, Houlsby GT, Martin CM, Zdravkovi L, et al. New design methods for large diameter piles under lateral loading for offshore wind applications. Front Offshore Geotech 2015;III:705–10.
[3] API. API Recommended Practice 2A-WSD Planning, Designing, and Constructing Fixed Offshore Platforms—Working Stress Design. 22nd ed.; 2014.
[4] DNV GL AS. DNVGL-ST-0126: support structures for wind turbines; 2016.
[5] Byrne B, McAdam R, Burd H, Houlsby G, Martin C, Beuckelaers W, et al. PISA: new design methods for offshore wind turbine monopiles. In: Proceeding offshore site investig geotech conf, London, UK; 2017.
[6] Burd H, Byrne B, McAdam R, Houlsby G, Martin C, Beuckelaers W, et al. Design aspects for monopile foundations. In: Proceeding 19th ICSMGE, Seoul; 2017.
[7] Fan C, Long J. Assessment of existing methods for predicting soil response of laterally loaded piles in sand. Comput Geotech 2005;32:274–89. http://dx.doi.org/10.1016/j.compgeo.2005.02.004.
[8] Lesny K, Paikowsky S, Gurbuz A. Scale effects in lateral load response of large diameter monopiles. In: Proc Sess Geo-Denver 2007 contemp issues deep found; 2007.
[9] Achmus M, Kuo Y-S, Abdel-Rahman K. Behavior of monopile foundations under cyclic lateral load. Comput Geotech 2009;36:725–35. http://dx.doi.org/10.1016/j.compgeo.2008.12.003.
[10] Bekken L. Lateral behaviour of large diameter offshore monopile foundations for wind turbines. Delft University of Technology; 2009.
[11] Kim Y, Jeong S. Analysis of soil resistance on laterally loaded piles based on 3D soil–pile interaction. Comput Geotech 2011;38:248–57. http://dx.doi.org/10.1016/j.compgeo.2010.12.001.
[12] Zdravković L, Taborda DMG, Potts DM, Jardine RJ, Sideri M, Schroeder FC. Numerical modelling of large diameter piles under lateral loading for offshore wind applications. In: Third int symp front offshore geotech (ISFOG 2015), Oslo Norway; 2015. p. 759–64.
[13] Gupta BK, Basu D. Analysis of laterally loaded rigid monopiles and poles in multilayered linearly varying soil. Comput Geotech 2016;72:114–25. http://dx.doi.org/10.1016/j.compgeo.2015.11.008.
[14] Thieken K, Achmus M, Lemke K. A new static p-y approach for piles with arbitrary dimensions in sand. Geotechnik 2015;38:267–88. http://dx.doi.org/10.1002/gete.201400036.
[15] Lesny K, Wiemann J. Finite-element-modelling of large diameter monopiles for offshore wind energy converters. GeoCongress 2006, Reston, VA: American Society of Civil Engineers; 2006. p. 1–6. http://dx.doi.org/10.1061/40803(187)212.
[16] Zdravković L, Taborda DMG, Potts DM, Jardine RJ, Sideri M, Schroeder FC, et al. Numerical modelling of large diameter piles under lateral loading for offshore wind applications. Front. Offshore Geotech. III, Oslo Norway; 2015. p. 759–64.
[17] Wang D, Bienen B, Nazem M, Tian Y, Zheng J, Pucker T, et al. Large deformation finite element analyses in geotechnical engineering. Comput Geotech 2015;65:104–14. http://dx.doi.org/10.1016/j.compgeo.2014.12.005.
[18] Khoa HDV, Jostad HP. Application of a cyclic accumulation model UDCAM to FE analyses of offshore foundations. In: Proc 4th Congrès Int Géotechnique – Ouvrages-Structures. CIGOS 2017; 2017. p. 656–67.
[19] Jostad HP, Grimstad G, Andersen KH, Sivasithamparam N. A FE procedure for calculation of cyclic behaviour of offshore foundations under partly drained conditions. Front Offshore Geotech III 2015. 978-1.
[20] Doherty P, Kirwan L, Gavin K, Igoe D, Tyrrell S, Ward D, et al. An overview of the UCD geotechnical research site at Blessington. In: Caprani C, O'Connor A, editors. Proc BCRI 2012, 6–7th Sept. 2012, Dublin, Dublin, Ireland: Bridge and Concrete Research Ireland; 2012. p. 499–504.
[21] Schanz T, Vermeer A, Bonnier P. The hardening soil model: formulation and verification. In: Beyond 2000 Comput Geotech 10 years PLAXIS Int Proc Int Symp beyond 2000 Comput Geotech Amsterdam Netherlands 1820 March 1999; 1999. p. 281.
[22] Bolton MD. The strength and dilatancy of Sands. Géotechnique 1986;36:65–78.
[23] Kulhawy F, Mayne PW. Manual on estimating soil properties for foundation design; 1990.
[24] Lunne T, Christoffersen HP. Interpretation of cone penetrometer data for offshore sands. In: 15th Annu OTC Houston, TX, May 2–5; 1983.
[25] Mayne PW, Kulhawy F. Ko – OCR relationships in soils. J Geotech Eng Div 1982;108:851–72.
[26] Mayne PW. Stress strain strength flow parameters from enhanced in-situ tests. In: Proceedings, Int Conf In-Situ Meas Soil Prop Case Hist. [In-Situ 2001], Bali, Indones; 2001. p. 27–48.
[27] Kulhawy F, Mayne PW. Manual on estimating soil properties for foundation design; 1990.
[28] Brinkgreve RBJ. PLAXIS 3D reference manual; 2013.
[29] Gavin K, O'Kelly B, Adekunte A. A field investigation of vertical footing response on sand. Proc ICE – Geotech Eng 2009;162:257–67. http://dx.doi.org/10.1680/geng.2009.162.5.257.
[30] Tolooiyan A, Gavin K. Modelling the cone penetration test in sand using cavity expansion and arbitrary Lagrangian Eulerian finite element methods. Comput Geotech 2011;38:482–90. http://dx.doi.org/10.1016/j.compgeo.2011.02.012.
[31] Igoe D, Gavin K, O'Kelly BC. Shaft capacity of open-ended piles in sand. J Geotech Geoenviron Eng 2011;137:903–13. http://dx.doi.org/10.1061/(ASCE)GT.1943-5606.0000511.
[32] Xue J, Murphy G, Doherty P, Igoe D, Gavin K. Optimization technique to determine the p-y curves of laterally loaded stiff piles in dense sand. Geotech Test J 2016;39:20140257. http://dx.doi.org/10.1520/GTJ20140257.
[33] Murphy G, Doherty P, Cadogan D, Gavin K. Field experiments on instrumented winged-monopiles. ICE Proc – Geotech Eng Press 2016;169:227–39. http://dx.doi.org/10.1680/jgeen.15.00134.
[34] Gavin KG. Behaviour of open and closed ended piles in sand – PhD Thesis. Trinity College Dublin; 1998.
[35] Phuong NTV, van Tol AF, Elkadi ASK, Rohe A. Numerical investigation of pile installation effects in sand using material point method. Comput Geotech 2016;73:58–71. http://dx.doi.org/10.1016/j.compgeo.2015.11.012.
[36] Dijkstra J, Broere W, Heeres OM. Numerical simulation of pile installation. Comput Geotech 2011;38:612–22. http://dx.doi.org/10.1016/j.compgeo.2011.04.004.
[37] Gavin K, Lehane BM. Estimating the end bearing resistance of pipe piles in sand using the final filling ratio. Front Offshore Geotech, Perth: Taylor and Francis; 2005. p. 717–24. http://dx.doi.org/10.1201/NOE0415390637.ch81.
[38] Dijkstra J, Broere W, van Tol AF. Eulerian simulation of the installation process of a displacement pile. contemp. top. situ testing, anal. reliab. found., Reston, VA: American Society of Civil Engineers; 2009, p. 135–42. http://dx.doi.org/10.1061/41022(336)18.
[39] Lam IP. Diameter effects on p-y curves. Deep mar found – a perspect des constr deep mar found; 2009, 88.